Laser and Particle Beams (2009), *27*, 291–296. Printed in the USA.
Copyright © 2009 Cambridge University Press 0263-0346/09 $20.00
doi:10.1017/S0263034609000391

Surface plasmon enhanced electron acceleration with few-cycle laser pulses

P. DOMBI, P. RÁCZ, AND B. BÓDI

Research Institute for Solid-State Physics and Optics, H-1121 Budapest, Konkoly-Thege M. út 29-33, Hungary

(RECEIVED 1 October 2008; ACCEPTED 29 January 2009)

Abstract

Surface plasmon enhanced electron acceleration is a recently discovered efficient particle acceleration phenomenon in the nanoscale-confined field of surface electromagnetic waves. For the generation and spatial/spectral control of keV-energy electrons generated, this way few-cycle laser pulses can be utilized particularly well. We present numerical results based on a simple model of this phenomenon analogous to the three-step model of high harmonic generation. We identify those parameter regimes where the emitted electron beam is highly directional and monoenergetic opening the door to novel ultrafast applications and methods.

Keywords: Electron acceleration; Few-cycle pulses; Surface plasmons; Ultrafast phenomena

1. INTRODUCTION

Ultrashort and intense laser pulses are particularly well suited for the generation of electron and other charged particle beams, both in the relativistic and in the non-relativistic regimes of laser-solid interactions (Malka, 2002; Irvine *et al.*, 2004; Gupta & Suk, 2007; Karmakar & Pukhov, 2007; Nickles *et al.*, 2007; Flippo *et al.*, 2007; Niu *et al.*, 2008; Chen *et al.*, 2008, and references therein). One of the methods to generate well-behaved electron beams with relatively low-intensity light pulses is surface plasmon enhanced electron acceleration. This phenomenon was discovered recently and it was experimentally demonstrated that it is suitable for the production of relatively high-energy, quasi-monoenergetic electron beams with the usage of simple femtosecond lasers (Zawadzka *et al.*, 2001; Kupersztych *et al.*, 2001; Irvine *et al.*, 2004). In this scheme, the evanescent electric field of surface plasmon polaritons (SPPs) accelerates photo-emitted electrons away from the surface. This process can be highly efficient so that keV kinetic energy levels can be reached with nJ-class oscillators without having to rely on external direct current fields (Irvine *et al.*, 2004; Irvine & Elezzabi, 2006). This method seems particularly advantageous for the generation of well-behaved femtosecond electron beams that can be used later on for infrared pump/electron probe methods, such as ultrafast electron diffraction or microscopy (Siwick *et al.*, 2003; Lobastov *et al.*, 2005). These novel time-resolved methods utilizing electron beams can gain importance in the future by enabling both high spatial and high temporal resolution material characterization at the same time. They will become particularly interesting if the attosecond temporal resolution domain becomes within reach, as suggested recently (Stockman *et al.*, 2007; Varró & Farkas, 2008; Fill *et al.*, 2006). Moreover, studying the spectral properties of femtosecond electron bunches has the potential to reveal ultrafast excitation dynamics in solids and provide the basis for a single-shot measurement tool of the carrier-envelope phase of ultrashort laser pulses, as we proposed recently (Irvine *et al.*, 2006; Dombi & Rácz, 2008). Other, carrier-envelope phase sensitive laser-solid interactions already demonstrated (Apolonski *et al.*, 2004; Dombi *et al.*, 2004, 2006; Fortier *et al.*, 2004; Mücke *et al.*, 2004) suffer from low experimental contrast, therefore it is necessary to look for higher contrast tools for direct phase measurement.

Motivated by these perspectives, it was shown numerically and partly also experimentally that surface plasmonic electron sources can be ideally controlled with ultrashort laser pulses so that they deliver highly directional, monoenergetic electron beams readily synchronized with the pump pulse (Irvine *et al.*, 2004, 2006; Dombi & Rácz, 2008). We developed a simple semiclassical approach for the simulation of this process that is analogous to the three-step model of high harmonic generation (Kulander *et al.*, 1993; Corkum, 1993). In this paper, we present the basic elements of this

Address correspondence and reprint requests to: Péter Dombi, Research Institute for Solid-State Physics and Optics, H-1121 Budapest, Konkoly-Thege M. út 29-33, Hungary. phone: +361 392 2222 ext. 3609. E-mail: dombi@szfki.hu

https://doi.org/10.1017/S0263034609000391 Published online by Cambridge University Press

model and show that it provides the same results as a much more complicated treatment of the problem based on the rigorous, but computationally time-consuming solution of Maxwell's equations. We also provide new insight into the spatiotemporal dynamics of SPP enhanced electron acceleration which is also important if one intends to realize adaptive emission control methods (Aeschlimann *et al.*, 2007).

2. THREE-STEP MODEL OF SPP ENHANCED ELECTRON ACCELERATION

SPP enhanced electron acceleration involves distinct physical processes such as (1) the coupling of the incident light and surface plasmonic electromagnetic fields, (2) the photoinjection of the electrons into vacuum from the metal layer, and (3) the subsequent acceleration of free electrons by the evanescent SPP field on the vacuum side of the surface. These steps represent an analogy with the semiclassical three-step model of high harmonic generation that can be used very efficiently to predict the outcome of atomic recollision processes (Kulander *et al.*, 1993; Corkum, 1993). This motivated us to adapt a more or less analogous model to the SPP environment where instead of a single atom, a solid surface is involved, which determines the conditions for recollision.

As a first step, we gained analytic formulae for SPP fields instead of the computationally intensive complete numerical solution of Maxwell's equations in the Kretschmann-Raether SPP coupling configuration used in previous studies (Irvine *et al.*, 2004). Based on the well-known fact that SPP fields decay exponentially away from the surface (Raether, 1988) we took an analytic expression for the SPP field components on the vacuum side of the metal layer in the form of

$$\mathrm{E}_y^{SPP}(x, y, \mathrm{t}) = \eta E_0 \mathrm{E}_{env}(x, t)\cos(k_{SPP}x - \omega_0 t + \varphi_0)\exp(-\alpha y) \quad (1)$$

$$\mathrm{E}_x^{SPP}(x, y, \mathrm{t}) = \eta a E_0 \mathrm{E}_{env}(x, t)\cos\left(k_{SPP}x - \omega_0 t - \frac{\pi}{2} + \varphi_0\right)\exp(-\alpha y) \quad (2)$$

where E_0 is the field amplitude, $\mathrm{E}_{\mathrm{env}}(x, t)$ is an envelope function determined by the temporal and spatial beam profiles of the incoming Gaussian pulse, η is the field enhancement factor resulting from SSP coupling (Raether, 1988), k_{SPP} is the SPP wave vector, ω_0 is the carrier frequency, φ_0 is the carrier-envelope phase of the laser pulse, and α is the inverse decay length of the plasmonic field in vacuum. For the accurate determination of the field, we used the evanescent decay parameter $\alpha = 247\ \mathrm{nm}^{-1}$ resulting from previous non-approximate studies carried out with the same input parameters for laser pulses having a central wavelength of 800 nm (Irvine *et al.*, 2006). We used the value of $a = 0.3$ according to the notion that the amplitudes of the x- and y-components of the plasmonic field have this ratio according to the numerical solution of Maxwell's equations (Irvine *et al.*, 2006). We concluded that the field given by Eqs. (1) and (2) approximates the exact SPP field with a very good accuracy by comparing our results to those of Irvine *et al.* (2006). One can examine the distribution of the field amplitude in the vicinity of the surface in Figure 1 (false color representation) showing very good agreement with the above-mentioned calculation and we also succeeded in reproducing the vector representation of the field depicted in Figure 3 in Irvine *et al.* (2006) with this method. The vector field that can be calculated with our model is depicted in the inset of Figure 1.

We then placed a point array along the prism surface and examined the spatial and temporal distribution of the photoemission (induced by the SPP field) along the surface, assuming field emission taking place at higher intensities. To this end, we applied the Fowler-Nordheim equation routinely used in studies involving electron emission from metal nanotips (Hommelhoff *et al.*, 2006; Ropers *et al.*, 2007). This describes the instantaneous tunneling current based on the fact that plasmonic fields carry substantial field enhancement factors (up to $\times 100$) compared to the generating field (Hommelhoff *et al.*, 2006; Ropers *et al.*, 2007). This way we gained a spatially and temporally resolved map of tunneling probabilities determined by the SPP field.

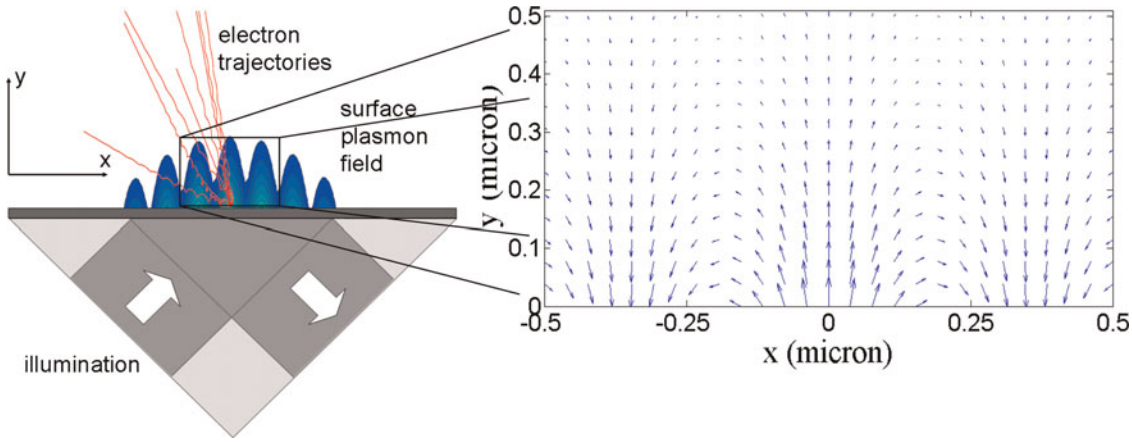


Fig. 1. (Color online) Illustration of the setup for the generation of electron beams by surface plasmon enhanced electron acceleration with field vectors and electron trajectories. See text for further details.

https://doi.org/10.1017/S0263034609000391 Published online by Cambridge University Press

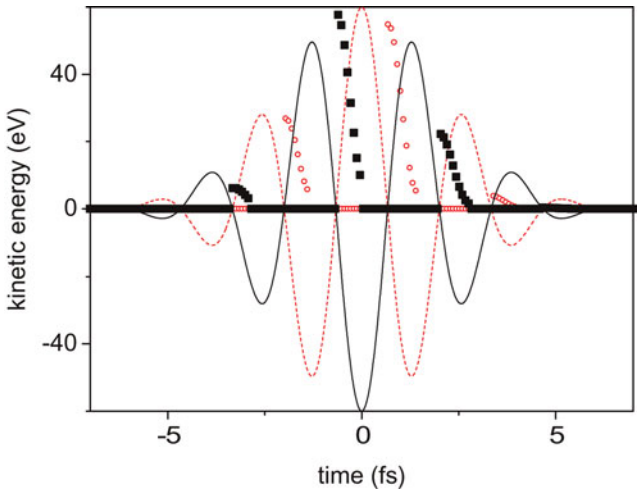


Fig. 2. (Color online) Surface plasmon accelerated electron energy as a function of the birth instant of the electrons (scatter plots). The plasmon generating 5 fs laser pulse (solid and dashed lines) has either a "cosine" (dashed curve) or "minus cosine" waveform (solid curve). Electron energies for the "cosine" waveform are depicted as circles, whereas for the "minus cosine" waveform, as squares. For further pulse parameters see text.

Third, we scrutinized the vacuum electron trajectories of photoemitted electrons in the plasmonic field for each point in the above-mentioned array and for several emission instants by solving free-electron equations of motions numerically. Some of these trajectories can be seen in Figure 1 (red curves). In some cases, the electron trajectories involved a recollision with the metal surface and when this happened, no electron emission was assumed. In all other cases, the final kinetic energies and directions of the photoemitted and photoaccelerated electrons were placed in a matrix for each emission point in space and for each emission instant. Figure 2 illustrates the temporal distribution of the final kinetic energies as a function of the electron "birth" instant for a maximum plasmonic field strength of 1.9×10^{11} V/m and for electrons emitted from the central part of the illuminated surface. The figure demonstrates similarities to the corresponding kinetic energy distributions of atomic electrons after being accelerated by the ionizing laser field (Reider, 2004). Here, it is important to note that roughly only one-fourth of the possible emission instants can contribute to the acceleration process. This is due to the symmetry breaking of the metal surface and the associated electron recollision and reabsorption processes.

3. DETERMINING MACROSCOPIC PROPERTIES OF THE ELECTRON BEAM

By integrating the above described emission maps along the spatial and/or temporal coordinates, macroscopic emission distributions and electron spectra can be calculated. First, we checked whether these reproduce former measurement and simulation results (Irvine *et al.*, 2004, 2006) to gain confidence in the simplified three-step model that we used. To this end, we carried out simulations for the same parameters as those published in Irvine and Elezzabi (2006*a*) and Irvine *et al.* (2006). For these simulations, we assumed multi-photon-induced electron emission (previously used in other simulations), which does not necessarily hold for higher intensities. However, our purpose in this case was to reproduce former results, therefore the temporal distribution of photoemission was described by $j(t, x) \sim I^n(t, x)$, where j is the photocurrent from the surface, I is the temporal intensity distribution of the SPP field along the surface, and n is the order of the multi-photon process. Here, $n = 3$ is used according to the 4.5–5 eV work function of most metals and the 1.5 eV photon energy at 800 nm. Figure 3a depicts macroscopic electron spectra gained with our model for peak plasmonic fields of 1.9×10^{11} V/m, 2.7×10^{11} V/m, and 3.7×10^{11} V/m, respectively (the full width at half maximum (FWHM) duration of the input Gaussian laser pulse was 30 fs with a central wavelength of 800 nm). Thereby, this figure can be directly compared to Figure 5 in Irvine *et al.* (2006). It can be seen that the characteristics of the electron spectra are very well reproduced, as well as the linear scaling of the kinetic energies of the most energetic electrons with intensity. Slight differences in the peak and cut-off positions can be attributed to the approximate nature of the SPP field expression used in our case as opposed to the numerical field solution used in Irvine *et al.* (2006).

In another comparative simulation, we changed the input pulse length to 5 fs FWHM, and assumed that this pulse is focused to a spot with 60 μm diameter on the prism surface. The field peak was 1.9×10^{11} V/m. In Figure 3b, we can see that the spectrum of the electron beam gained this way reproduces the spectrum computed with other methods, such as the one in Figure 1b in Irvine *et al.* (2006). Slight differences in the cut-off positions can still be observed, however, all spectral features and the position of the main peak are exactly the same. Therefore the applicability of the analytic field expressions (Eqs. (1) and (2)) and the robustness of our approach was confirmed by these examples.

We can now turn attention to modeling electron spectra by assuming field emission from the metal surface, which is a more realistic assumption for higher intensity input beams, approaching the damage threshold of thin metal films. High repetition-rate, ultrafast laser output delivering focused intensity in this range is achievable with simple Ti:sapphire oscillators with an extended cavity, as we demonstrated it recently (Naumov *et al.*, 2005; Dombi & Antal, 2007; Dombi *et al.*, 2007). We then used the Fowler-Nordheim formula, as described above, and both angularly and spectrally resolved the photoaccelerated electron beam, assuming a maximum input field of 5.8×10^{10} V/m, which is a rather realistic maximum value considering the damage threshold of gold and silver films. We also assumed a tunneling time of 600 attosecond, which in our model, describes the delay between the actual distortion of the potential by the field and the corresponding appearance

https://doi.org/10.1017/S0263034609000391 Published online by Cambridge University Press

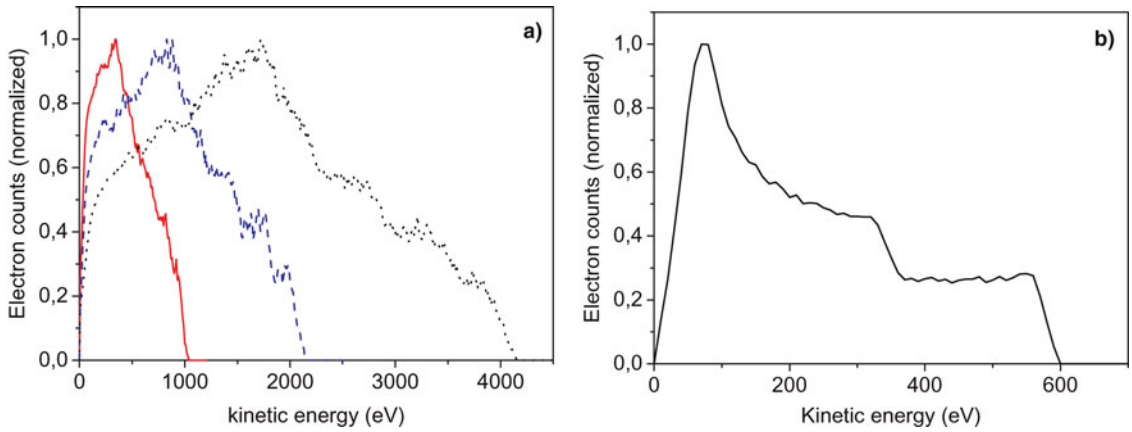


Fig. 3. (Color online) (**a**) Macroscopic electron spectra at peak plasmonic fields of 1.9×10^{11} V/m (solid line), 2.7×10^{11} V/m (dashed line), and 3.7×10^{11} V/m (dotted line) for a Gaussian input laser pulse of 30 fs FWHM duration with a central wavelength of 800 nm). (**b**) Electron spectrum for a 5 fs generating pulse with a peak plasmonic field strength of 1.9×10^{11} V/m, assuming multi-photon photoemission.

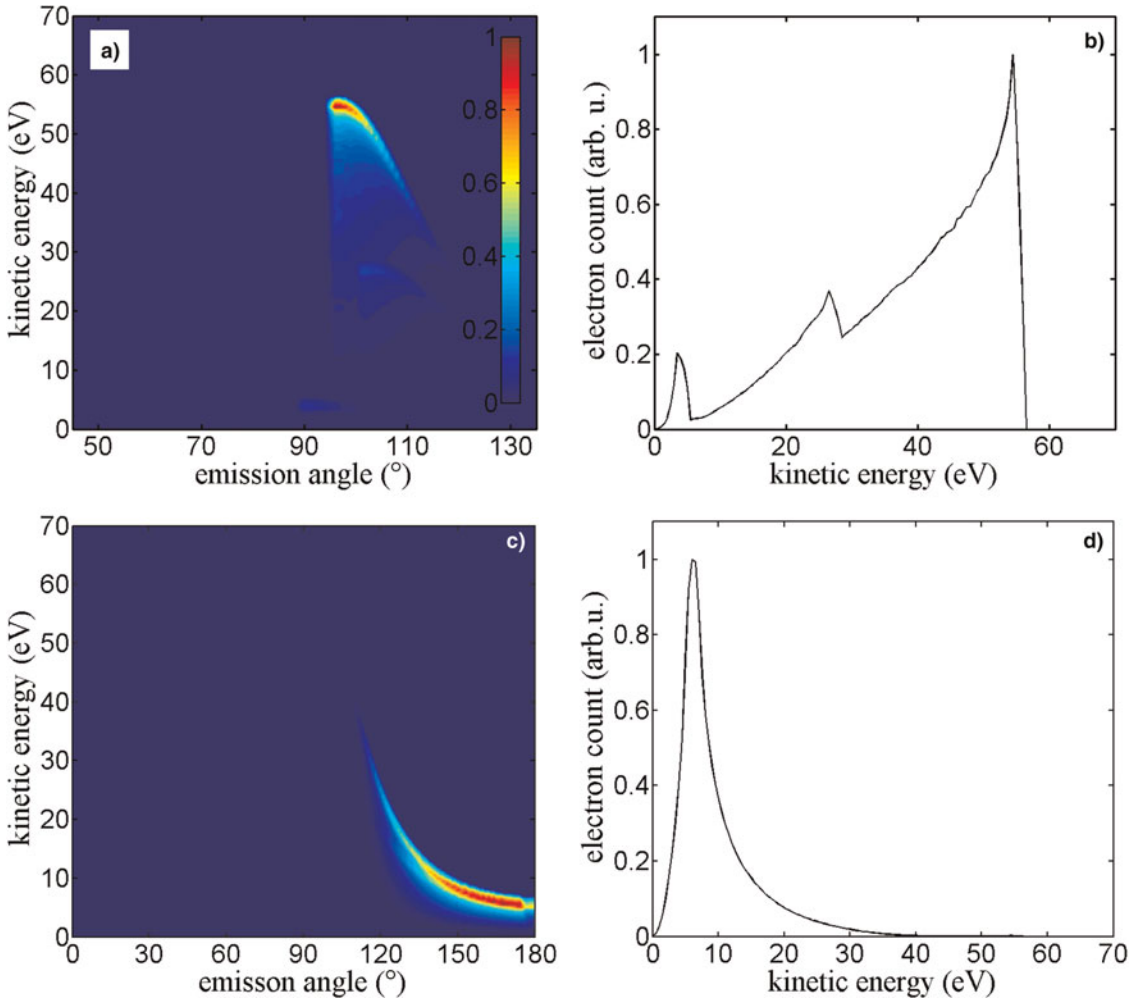


Fig. 4. (Color online) Angular and kinetic energy distribution (**a** and **c**) and macroscopic electron spectrum (**b** and **d**) of surface plasmon accelerated electrons for 5 fs FWHM laser pulses and a maximum field strength of 5.8×10^{10} V/m, assuming tunneling emission from the surface with 600 as (a and b) and 150 as delay (c and d) with respect to the SPP electric field.

https://doi.org/10.1017/S0263034609000391 Published online by Cambridge University Press

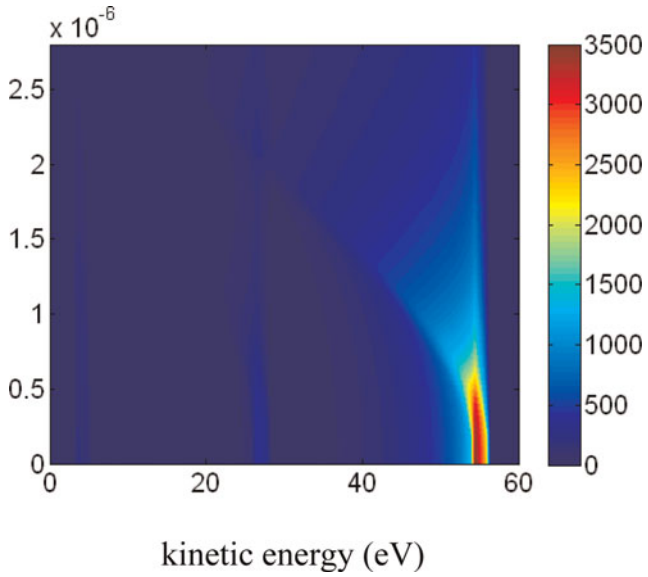


Fig. 5. (Color online) Kinetic energy distribution of SPP accelerated electrons emitted from a nano-confined window for a maximum field strength of 5.8×10^{10} V/m as a function of the size of the window (y-axis, in meters). See text for further details.

of the electron in the continuum. The simulation results can be seen in Figure 4a with false color representation of the electron count value as a function of energy and emission angle. It can be seen that the electron beam is highly directional, most of it being emitted to the $95^\circ - 105^\circ$ angular range. The beam has also acquired a quasi-monoenergetic feature as it can be seen in Figure 4b. This spectrum is generated by integrating the angular-energy distribution along the angular axis. The quasi-monoenergeticity of the spectrum is a significant difference as compared to the case in Figure 3b, and can be attributed exclusively to the different emission regimes (multiphoton *versus* tunneling) involved. The sharp temporal distribution of the tunneling peaks located at the field maxima favor the emission of electrons at those time instants when they can gain significant kinetic energy. The sharp spectral drop corresponds to the highest energy electrons in the multiphoton case. But it is mostly these electrons that are represented in the field emission case; therefore, it appears as a sharp cut-off in the spectrum. The low-energy wing of the spectrum, however, displays a broader feature, making the source less suitable for ultrafast applications. Figures 4c and 4d display calculations assuming a tunneling time of 150 as, otherwise, the parameters are unchanged. It can be seen that high-energy electrons are considerably suppressed and the advantageous quasi-monoenergetic feature of the spectrum also disappears. Hence, the actual value of the tunneling time (depending on the field strength, the work function, and the length of the optical cycle) has a decisive influence on the acceleration process. As it is a significant challenge to measure this delay in the field emission process (Eckle *et al.*, 2008) and in spite of the rapid development of attosecond techniques, there is no corresponding measurement for metals that we are aware of, we can only state that this value lies closer to one-fourth of the optical cycle duration for the field strengths concerned. This value can be derived with density functional methods (Lemell *et al.*, 2003) as well as from simple quantum mechanical considerations.

To generate spectra with higher monoenergeticity, we suggest the application of spatial confinement of the emission area on the metal surface. Experimentally, this can be carried out by various nanofabrication techniques, e.g., by depositing a dielectric layer on top of the metal with a nanoscale opening where the dielectric overlayer is absent and the metal surface is exposed to vacuum. Another possibility is roughening a small rectangular area on top of the metal surface thereby enhancing the emission from that portion of the film. These potential schemes were taken into account in our simulations by selecting only smaller areas of the surface illuminated by the laser beam and considered only those photoelectrons that were emitted from this area. Then, we determined macroscopic spectra as a function of the radius of the nano-opening, and depicted these normalized distributions in false color representation in Figure 5. One sees that limiting the emission area clearly improves the monoenergetic nature of the electron beam, as depicted in Figure 5. According to the figure, we can determine that the ideal size of the opening is around 200–500 nm. The spectral monoenergeticity is highly improved in this range and the escape area is not too small to allow a significant photoelectron escape.

4. SUMMARY

We modeled few-cycle pulse-induced, SPP enhanced electron acceleration with a semiclassical approach similar to the three-step model of high harmonic generation. Our analytic approximation for the plasmonic field enables the reproduction of former results gained by the direct, but very processor time consuming solution of Maxwell's equations. We have shown that this phenomenon can serve as a basis for an ultrafast, monoenergetic electron source with a spectrum peaking at hundreds of eVs. It is anticipated that even higher degrees of monoenergeticity can be reached by applying a nano-sized window on the emission area. Thereby, the surface plasmonic acceleration scheme can provide a solution for novel time-resolved diffraction methods and serve as a basis for time-resolved studies of ultrafast surface processes.

REFERENCES

Aeschlimann, M., Bauer, M., Bayer, D., Brixner, T., García de Abajo, F.J., Pfeiffer, W., Rohmer, M., Spindler, C. & Steeb, F. (2007). Adaptive subwavelength control of nano-optical fields. *Nat.* **446**, 301–304.

Apolonski, A., Dombi, P., Paulus, G.G., Kakehata, M., Holzwarth, R., Udem, T., Lemell, C., Torizuka, K., Burgdörfer, J., Hänsch, T.W. & Krausz, F. (2004).

https://doi.org/10.1017/S0263034609000391 Published online by Cambridge University Press

Observation of light-phase-sensitive photoemission from a metal. *Phys. Rev. Lett.* **92**, 073902.

Chen, Z.L., Unick, C., Vafaei-Najafabadi, N., Tsui, Y.Y., Fedosejevs, R., Naseri, N., Masson-Laborde, P.E. & Rozmus, W. (2008). Quasi-monoenergetic electron beams generated from 7 TW laser pulses in N-2 and He gas targets. *Laser Part. Beams* **26**, 147–155.

Corkum, P.B. (1993). Plasma perspective on strong-field multiphoton ionization. *Phys. Rev. Lett*. **71**, 1994–1997.

Dombi, P., Apolonski, A., Lemell, C., Paulus, G.G., Kakehata, M., Holzwarth, R., Udem, T., Torizuka, K., Burgdörfer, J., Hänsch, T.W. & Krausz, F. (2004). Direct measurement and analysis of the carrier-envelope phase in light pulses approaching the single-cycle regime. *New J. Phys*. **6**, 39.

Dombi, P., Krausz, F. & Farkas, G. (2006). Ultrafast dynamics and carrier-envelope phase sensitivity of multiphoton photoemission from metal surfaces. *J. Mod. Opt*. **53**, 163–172.

Dombi, P. & Antal, P. (2007). Investigation of a 200 nJ Ti:sapphire oscillator for white light generation. *Laser Phys. Lett*. **4**, 538–542.

Dombi, P., Antal, P., Fekete, J., Szipöcs, R. & Várallyay, Z. (2007). Chirped-pulse supercontinuum generation with a long-cavity Ti:sapphire oscillator. *Appl. Phys. B* **88**, 379–384.

Dombi, P. & Rácz, P. (2008). Ultrafast monoenergetic electron source by optical waveform control of surface plasmons. *Opt. Express* **16**, 2887–2893.

Eckle, P., Pfeiffer, A., Cirelli, C., Staudte, S., Dörner, R., Muller, H.G., Büttiker, M. & Keller, U. (2008). Attosecond ionization and tunneling delay time measurements. *Sci* **322**, 1525–1529.

Fill, E., Veisz, L., Apolonski, A. & Krausz, F. (2006). Sub-fs electron pulses for ultrafast electron diffraction. *New J. Phys*. **8**, 272.

Flippo, K., Hegelich, B.M., Albright, B.J., Yin, L., Gautier, D.C., Letzring, S., Schollmeier, M., Schreiber, J., Schulze, R. & Fernandez, J.C. (2007). Laser-driven ion accelerators: Spectral control, monoenergetic ions and new acceleration mechanisms. *Laser Part. Beams* **25**, 3–8.

Fortier, T.M., Roos, P.A., Jones, D.J., Cundiff, S.T.R., Bhat, R.D. & Sipe, J.E. (2004). Carrier-envelope phase-controlled quantum interference of injected photocurrents in semiconductors. *Phys. Rev. Lett*. **92**, 147403.

Gupta, D.N. & Suk, H. (2007). Electron acceleration to high energy by using two chirped lasers. *Laser Part. Beams* **25**, 31–36.

Hommelhoff, P., Kealhofer, C. & Kasevich, M.A. (2006). Ultrafast electron pulses from a tungsten tip triggered by low-power femtosecond laser pulses. *Phys. Rev. Lett*. **97**, 247402.

Irvine, S.E., Dechant, A. & Elezzabi, A.Y. (2004). Generation of 0.4-keV femtosecond electron pulses using impulsively excited surface plasmons. *Phys. Rev. Lett*. **93**, 184801.

Irvine, S.E. & Elezzabi, A.J. (2006). Surface-plasmon-based electron acceleration. *Phys. Rev. A* **73**, 013815.

Irvine, S.E., Dombi, P., Farkas, G. & Elezzabi, A.Y. (2006). Influence of the carrier-envelope phase of few-cycle pulses on ponderomotive surface-plasmon electron acceleration. *Phys. Rev. Lett*. **97**, 146801.

Karmakar, A. & Pukkov, A. (2007). Collimated attosecond GeV electron bunches from ionization of high-Z material by radially polarized ultra-relativistic laser pulses. *Laser Part. Beams* **25**, 371–377.

Kulander, K.C., Schafer, K.J. & Krause, J.L. (1993). *Dynamics of Short-Pulse Excitation, Ionization and Harmonic Conversion*. New York: Plenum.

Kupersztych, J., Monchicourt, P. & Raynaud, M. (2001). Ponderomotive acceleration of photoelectrons in surface-plasmon-assisted multiphoton photoelectric emission. *Phys. Rev. Lett*. **86**, 5180–5183.

Lemell, C., Tong, X.-M., Krausz, F. & Burgdörfer, J. (2003). Electron emission from metal surfaces by ultrashort pulses: Determination of the carrier-envelope phase. *Phys. Rev. Lett*. **90**, 076403.

Lobastov, V.A., Srinivasan, R. & Zewail, A.H. (2005). Four-dimensional ultrafast electron microscopy. *Proc. Nat. Acad. Sci*. **102**, 7069–7073.

Malka, V. (2002). Charged particle source produced by laser-plasma interaction in the relativistic regime. *Laser Part. Beams* **20**, 217–221.

Mücke, O.D., Tritschler, T., Wegener, M., Morgner, U., Kärtner, F.X., Khitrova, G. & Gibbs, H.M. (2004). Carrier-wave Rabi flopping: role of the carrier-envelope phase. *Opt. Lett*. **29**, 2160–2162.

Naumov, S., Fernandez, A., Graf, R., Dombi, P., Krausz, F. & Apolonski, A. (2005). Approaching the microjoule frontier with femtosecond laser oscillators. *New. J. Phys*. **5**, 216.

Nickles, P.V., Ter-Avetisyan, S., Schnuerer, M., Sokollik, T., Sandner, W., Schreiber, J., Hilscher, D., Jahnke, U., Andreev, A. & Tikhonchuk, V. (2007). Review of ultrafast ion acceleration experiments in laser plasma at Max Born Institute. *Laser Part. Beams* **25**, 347–363.

Niu, H.Y., He, X.T., Qiao, B. & Zhou, C.T. (2008). Reasonant acceleration of electrons by intense circularly polarized Gaussian laser pulses. *Laser Part. Beams* **26**, 51–59.

Raether, H. (1988). *Surface Plasmons on Smooth and Rough Surfaces and on Gratings*. New York: Springer.

Reider, G. (2004). XUV attosecond pulses: Generation and measurement. *J. Phys. D* **37**, R37–R48.

Ropers, C., Solli, D.R., Schulz, C.P., Lienau, C. & Elsaesser, T. (2007). Localized multiphoton emission of femtosecond electron pulses from metal nanotips. *Phys. Rev. Lett*. **98**, 043907.

Siwick, B.J., Dwyer, J.R., Jordan, R.E. & Miller, R.J.D. (2003). An atomic-level view of melting using femtosecond electron diffraction. *Sci*. **302**, 1382–1385.

Stockman, M., Kling, M.F., Krausz, F. & Kleineberg, U. (2007). Attosecond nanoplasmonic field microscope. *Nat. Photon*. **1**, 539–544.

Varró, S. & Farkas, G. (2008). Attosecond electron pulses from interference of above-threshold de Broglie waves. *Laser Part. Beams* **26**, 9–20.

Zawadzka, J., Jaroszynski, D., Carey, J.J. & Wynne, K. (2001). Evanescent-wave acceleration of ultrashort electron pulses. *Appl. Phys. Lett*. **79**, 2130–2132.

https://doi.org/10.1017/S0263034609000391 Published online by Cambridge University Press